生命グローバル COE 若手研究成果発表会

「生命時空間ネットワーク進化型教育研究拠点」

THE RESEARCH ACHIEVEMENTS OF GCOE PROGRAM

"EVOLVING EDUCATION AND RESEARCH CENTER FOR SPATIO-TEMPORAL BIOLOGICAL NETWORK"

1 月 27 日(金) すずかけ台キャンパス すずかけホール

PROGRAM

10:00	**Opening:**	**Prof. Makio Tokunaga (GCOE Program Leader)**	
10:15 – 11:45	**GCOE Research Assistants' Oral Presentation**		
	10:15-10:25	O1: Takamura, Tsukasa	C2: Sandhu Lab
	10:25-10:35	O2: Ishikawa, Ryosuke	C2: Sandhu Lab
	10:35-10:45	O3: Tanno, Hidetaka	C3: Komada Lab
	10:45-10:55	O4: Ito, Hidehiro	C2: Kamachi Lab
	10:55-11:05	O5: Nagasaka, Kota	C1: Hirota Lab (Cancer Institute)
	11:05-11:15	O6: Islam, Zinia	C1: Hirose Lab
	11:15-11:25	O7: Gallegopaez, Lina	C1: Shirahige Lab (Tokyo Univ.)
	1125-11:35	O8: Jovic, Dragomirka	C3: Akaike Lab
	11:35-11:45	O9: Yazawa, Kenjiro	C2: Okahata Lab
12:00 – 13:00	**Break**		
13:00 – 15:00	**GCOE Assistant Professors' Oral Presentation**		
	13:00-13:20	Ando, Hideki	Handa Lab
	13:20-13:40	Kobayashi, Kenji	Kishimoto Lab
	13:40-14:00	Tsunoda, Hirosuke	Sekine Lab
	14:00-14:20	Terai, Yohey	Okada Lab
	14:20-14:40	Nemoto, Yasuhiro	Watanabe Lab
	14:40-15:00	Hexig, Bayar	Akaike Lab
15:00 – 17:00	**GCOE Research Assistants' Poster Presentation**		
17:00 – 20:00	**Award Ceremony & Banquet**		

※出席される方には投票用紙を配布します。皆様の投票数によって　研究科長賞を決定致します※
奮って　ご参加ください。

Contact: 生命理工学研究科 GCOE 拠点事務室
Tel: 045-924-5930 (x5930)
Email: gcoe-bio@bio.titech.ac.jp

<Award>

Prize Winner(s) will be selected by your ballot!

<< Oral Presentation>>

1 x Dean's best award

3 x Dean's award

<< Poster Presentation>>

1 x Dean's poster award (Gold)

1 x Dean's poster award (Silver)

5 x Dean's poster award (Blonze)

**** For Oral Presenters***

- Go to the reception and receive your name tag prior to your presentation.

- Set up your computer upon entering

- Await your turn

**** For all Poster Presenters***

- Lounge will be open from 9:00.

- Must check in at the reception & display your poster on the board by 13:00.

- Presentation number will be attached on the top of the board.

*** We do not have any pins for posters. Please bring your own.*

**** For all Audiences/Voters***

- Check in at the reception & receive the ballot(s)

- Ballots; 3 points for Professors/1 point for students

- Participate in the presentation and select the best presenter(s).

- Prize Winners will be selected and announced during the ceremony.

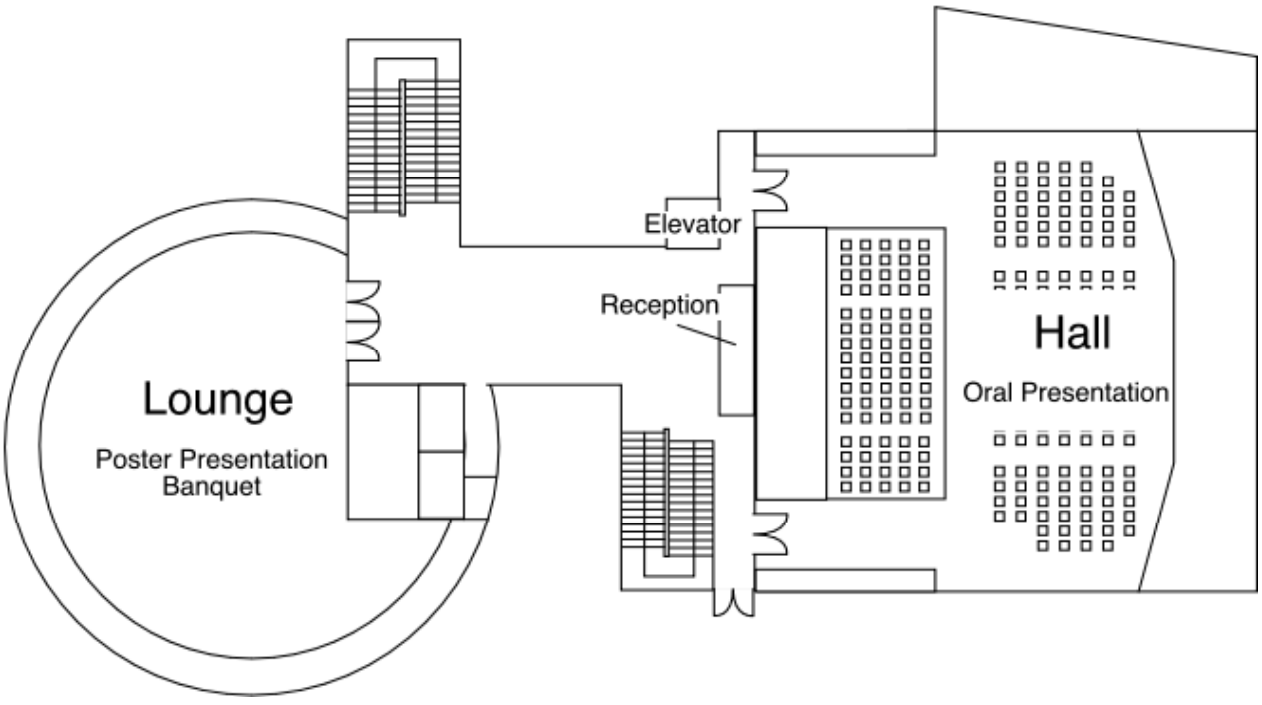

Global COE Research Assistants' ORAL Presentation

FOR

Dean's Award

10:15 ～

Planar Microfluidic System based on Electrophoresis for Detection of 130-nm Magnetic Lables for Biosensing

Takamura, Tsukasa

Cluster 2

There is increasing interest in the development of medical diagnostics based on the detection of functionalized superparamagnetic beads (SPBs) for fast, high sensitivity, and inexpensive point of care protocols. Portable biosensing systems based on such ‘magnetic labels’ are expected to find wide ranging applications for the diagnosis of heart disease and monitoring drivers under the influene of illegal drugs. In present day approaches, 200- and 3000-nm-diameter “magnetic labels” are usually detected using giant magnetoresistance and spin valve sensors, or Hall effect devices. However, demands for improvements in quantification, biomolecular affinity, and accuracy, necessitate the use of sub-200 nm magnetic labels. The main hurdle limiting the use of sub-200 nm beads is the difficulty in detecting small concentrations of such small magnetic labels using magnetoresistative-based sensors.

In order to overcome these limitations of giant magnetoresistance and Hall sensors, we have developed a simple procedure based on the detection of 130-nm target magnetic beads immobilized on substrates via the self-assembly and capture of micro-sized superparamagnetic ‘columnar beads’ by the targets. The optical observation of magnetically self-assembled columnar beads implies the existence 130 nm target magnetic beads which are not otherwise detectable either optically or electrically. The micrometer sized superparamagnetic beads we used consist of nanometer sized magnetic beads such as Fe3O4, typically 5–10 nm in diameter embedded in a polystyrene matrix.

Irrespective of the method used for detecting magnetic labels, a complete diagnostic system necessitates the integration of the sensors with microfluidic channels. Now, conventional microfluidic device consist of microfluidic channels—etched in glass—attached to external pumps for pushing solutes over the sensors. The use of large bulky external pumps is not conducive for portable, point of care systems.

In our study we demonstrated a novel biosensing systems exploiting the advantages of magnetic labels, and integrated with ‘planar’ microchannels produced without etching and which do not require external pumps. Furthermore, our pump-free system does not require peripheral tubes, thereby making it suitable for POCT applications. In our pumpless system, micrometer sized columnar beads were manipulated by an external electric field and captured by magnetic dipole interaction with the target beads immobilized on substrates. The movement and capture of the columnar beads by the target beads in liquid microchannels was clearly visible under an optical microscope even though the target beads were unobservable optically or detectable by magnetoresistive sensors.

We realized a biosensing protocol based on monitoring the electrostatic manipulation and magnetic capture of 1μm-diameter superparamagnetic columnar beads by 130-nm-diameter target beads in pumpless liquid microchannels. Our experimental setup was simple, and the procedure has potential for the rapid detection of extremely low concentrations of magnetically labelled biomolecules.

10:25 ～

Chemically derived graphene for optically transparent and electrically conducting thin films

Ishikawa, Ryosuke

Cluster 2

Interestingly, although Chemically derived graphene is itself fluorescent, it can also quench fluorescence. These seemingly contradictory properties are a manifestation of the heterogeneous chemical, atomic and electronic structures of chemically derived graphene. Recently several biological applications using the versatile optical properties of GO have emerged.

The final goal of this study is to develop high-performance graphene based transparent and conducting films (TCFs) for bio-applications. Chemically derived graphene is synthesized and functionalized for serving this goal. Since the synthetic process affects on the performance of obtained graphene thin films, to develop an optimized route of synthesis is quite important as a first step. Moreover, another key factor governing the performance of graphene based TCFs is deposition method utilizing synthesized graphene flakes. To suppress the inter-flake resistance is required for achieving a high performance TCFs. For this purpose, an attractive deposition method based on a new concept is investigated. In addition, the carrier doping technique is another emerging issue not only for the TCFs application but also for other device applications. The performance of graphene based thin films can be enhanced by modulation of carrier concentration.

(i) First of all, synthesis and characterization of chemically derived graphene was demonstrated. Chemically derived graphene was converted from graphene oxide (GO) in this study. As a first step, graphite was oxidized and exfoliated into GO by modified Hummers method and using mixed acid. AFM measurement and Raman spectroscopic study found that obtained dispersion includes monolayer and a few layers of GO flakes with lateral dimensions exceeding 150 μm. Because electrical conductivity can be recovered by restoring the π-network, one of the most important reactions of GO is its reduction. Therefore liquid phase reduction was attempted in addition to conventional reduction methods such as gaseous hydrazine and high-vacuum annealing. XPS data indicated that liquid phase reduction achieves almost same recovery of sp^2 network as conventional reduction process without any vacuum system. The patterning process of GO on silicone substrate enables fabrication of graphene devices simultaneously on substrate. Electrical transport property of synthesized graphene flakes was measured by utilizing fabricated devices structure. The electron mobility of monolayered reduced GO flake was determined to be as high as 10 $cm^2\ V^{-1}\ s^{-1}$. Then, graphene thin films were deposited by drop-casting, spin-casting, and spray-casting methods as conventional deposition methods. Both drop casting and spin-casting resulted in aggregation of GO flakes in which some places on the substrate was total absence of GO flakes. However, for spray-casting, the coverage was higher compared to aforementioned two methods, although minor aggregation of flakes was observed. Transmittance and sheet resistance were decreased linearly by changing spray volume, which indicated film thickness can be controlled by spray volume. Although the carrier mobility of individual RGO flakes was much higher than that of previous reports, the sheet resistance of fabricated RGO films was far from the requirement for real application to transparent conductive films.

(ii) Synthesis of amine-functionalized GO was intended for its utilization in layer-by-layer (LBL) assembly of GO for fabrication of transparent conductive film. Spectroscopic observations showed the presence of ethylenediamine (EDA) attached to GO. The challenging aspect of solution-process of graphene was the aggregation of graphene flakes upon the evaporation of solvent, which prevents the formation of uniform thin film. Alternatively, LBL assembly of graphene oxide was utilized to fabricate graphene-based thin film in a scalable and highly reproducible way.

It was found that optical transmittance and sheet resistance of the film decreases with an increase in number of LBL cycles in a reproducible way. The sheet resistance of LBL-assembled GO film decreases by an order of magnitude at the same optical transparency. That of resulting LBL-assembled GO film was 24 $k\Omega\ sq.^{-1}$ at optical transmittance of around 80% with light wavelength of 550 nm. Investigated LBL assembly method showed a high-potential of graphene-based TCFs for a wide field of application.

(iii) A novel method for the carrier doping of graphene using radical-assisted conjugated organic molecules in the liquid phase was investigated. This doping method is based on charge transfer interaction between the radicalized tetracyanoquinodimethane (TCNQ) molecule in specific organic solvent and chemically derived graphene flakes. The degree of charge transfer, *Z*, was estimated at 0.39 from the C≡N vibration frequency in Raman shift. By comparing the estimated *Z* value (0.2 ~ 0.3) of TCNQ/CNT system from ab initio calculations, much higher Z value of TCNQ/RGO indicates stronger interaction between TCNQ and RGO. The change in the surface work function might be mainly caused by the Fermi level (E_F) shifting towards the Dirac point (E_D) due to hole-doping from TCNQ via charge transfer. Due to carrier doping via the charge transfer interaction from TCNQ, the sheet resistance of the doped graphene films drastically decreased by two orders of magnitude without significant degradation of the optical transparency as a result of increasing the sheet carrier density from 1.02 x 10^{10} cm^{-2} to 1.17 x 10^{12} cm^{-2}. Finally, stability of doping effect with time evolution at room temperature under ambient atmosphere was monitored. R_s increased by less than 10 % after 1 year. Moreover, the doping effect indicated higher thermal stability than F4-TCNQ. Those stabilities are quite critical issue of doping technique in any application fields. The doped chemically-derived graphene films via radical-assisted chemical doping have huge potential as an alternative material for transparent conductive films in low-cost and low-temperature processes.

As mentioned above, mainly three important key technologies for improving the performance of graphene based TCFs were established in this study as noted below, (i) effective reduction process in liquid phase, (ii) novel large-area deposition method based on layer-by-layer assembly, and (iii) effective and stable carrier doping method via charge transfer.

10:35 ～

The Ankrd13 family of UIM-bearing proteins regulates EGF receptor endocytosis from the plasma membrane

Tanno, Hidetaka

Cluster 2

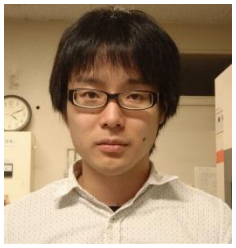

Ubiquitin is a 76-amino acid (a.a.) protein highly conserved in eukaryotic cells. Via the C-terminal carboxyl group, ubiquitin is conjugated to the ε-amino group of Lys residues in numerous intracellular proteins, a post-translational modification referred to as monoubiquitination. Ubiquitin is also conjugated to one of seven Lys residues or the N-terminal group in another ubiquitin molecule, forming eight structurally-different polyubiquitin chains. Among them, Lys48- and Lys63-linked chains are most abundant in the cell. Target proteins are often conjugated with polyubiquitin chains, and this modification is referred to as polyubiquitination. The fate or function of ubiquitinated proteins is regulated in different ways depending on the linkage pattern of conjugated ubiquitin.

On the plasma membrane, mono ubiquitin and/or Lys63-linked polyubiquitin chains serve as an endocytosis (internalization) signal that is tagged to a variety of cell surface integral membrane proteins in yeast and mammalian cells. The role of ubiquitin in endocytosis, however, is more complicated because not only cargo proteins but also proteins of the endocytic machinery are regulated by their own ubiquitination.

Epidermal growth factor (EGF) receptor (EGFR), belonging to the receptor tyrosine kinase family in mammals, is a cell surface protein whose mechanisms of endocytosis have been studied extensively. Following stimulation with EGF, EGFR undergoes rapid ubiquitination (mainly Lys63-linked polyubiquitination) by the Cbl family of Ubiquitin ligases. Inhibition of the Cbl activity results in suppressed internalization of ligand-activated EGFR. By contrast, in-frame fusion of Ubiquitin to the C-terminal cytoplasmic tail of EGFR induces its internalization in the absence of ligand. These observation suggest that ubiquitination serves as a trigger that drives endocytosis of EGFR from the cell surface.

The ubiquitin interacting motif (UIM) is a ~20 a.a sequence that specifically binds to ubiquitin. UIMs are found in multiple proteins involved in endocytic trafficking. Among UIM-bearing proteins, epsin and eps15 participate in the clathrin-mediated endocytosis of ubiquitinated cell surface proteins. But the mechanism of ubiquitin-dependent endocytosis of cell surface proteins is not completely understood.

Here, we examined the role of the ankyrin repeat domain (Ankrd) 13A, 13B, and 13D proteins, which constitute a functionally unknown family of UIM-bearing proteins, in the ubiquitin dependent-endocytosis. Stimulation of human HeLa cells with EGF rapidly induced direct binding of Ankrd 13 proteins to ubiquitinated EGFR via the UIMs. Ankrd 13 proteins bound specifically to Lys63-linked ubiquitin chains, which was consistent with a previous report that EGFR mainly undergoes Lys63-linked polyubiquitination. Ankrd 13 proteins were anchored, via the central region and UIMs, to the plasma membrane where they co-localize with EGFR. Finally, overexpression of wild-type as well as truncated-mutant Ankrd 13 proteins strongly inhibited rapid endocytosis of ubiquitinated but not unmodified EGFR from the surface in EGF-treated cells. We conclude that by binding to the Lys63-linked polyubiquitin moiety of EGFR at the plasma membrane, Ankrd 13 proteins facilitate the rapid internalization of ligand-activated EGFR

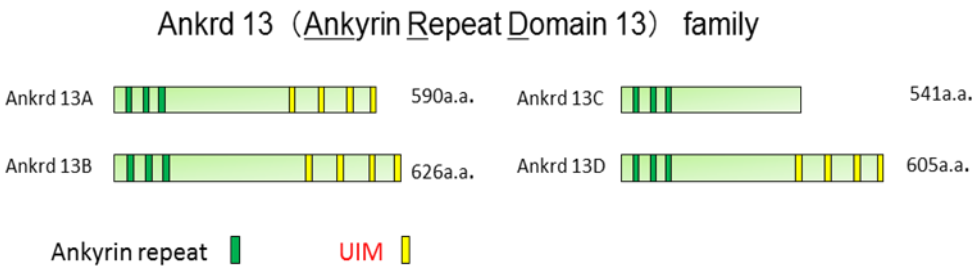

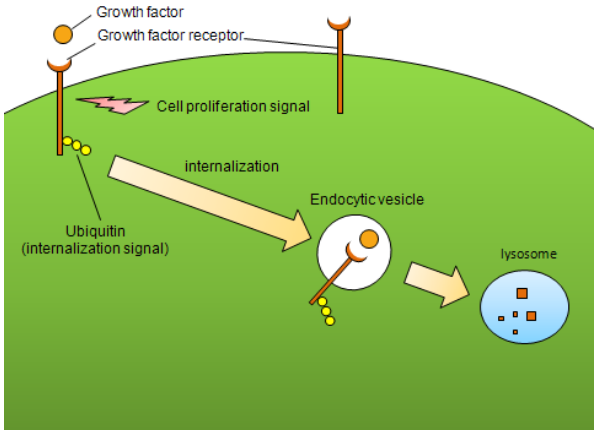

10:45 ～

Preparation of an article vesicle for chemical energy production by using light energy

Ito, Hidehiro

Cluster 2

The biological membrane plays a role as a physical barrier that maintains the integrity of the cell. In addition to its role, the biological membrane provides many functions necessary for the biological activities, including acquisition of nutrients and energy sources, reproduction, cellular recognition, and so on. The important point to carry out these functions is the modification of lipid bilayer membrane with proteins and carbohydrates.

Recently, functionalization of vesicle by the modification various functional group, including biological molecules, is one of the most active topics. These researches require an efficient and convenient method for introducing functional ligands onto the surface of vesicle. However, there are not any reports on the specific modification of inner or outer surface of vesicle. On the other hand, glycolipids are one of the major components of cellular membranes and comprise 90 % of thylakoid membranes, where the photosynthetic reactions occur. However, relatively few works have focused on the vesicle formation using glycolipids compared with phospholipids. First we report a method for the specific modification of inner or outer surface of the glycolipid vesicle. The surface modification was achieved by a copper(I) catalyzed 1,3-dipolar cycloaddition of azides and alkynes, which is a typical reaction of click chemistry.

We synthesized the glycolipid **1** which has an acetylene part for modification by click chemistry. The preparation of unilamellar vesicles using the glycolipid **1** was carried out under sonication. The average diameter of the vesicle was obtained about 100 nm by TEM and DLS.

We prepared the glycolipid **1** vesicle solution containing two azido compounds, one is located in the internal aqueous phase and the other one is in the outside vesicle. When the copper(I) catalyst was added in the outside vesicle, the modification was only carried out at the outer surface of the vesicle by observed from ESI-MS measurement. To achieve the specific modification of inner surface of the glycolipid **1** vesicle, we used the photoresponsive copper complex [Cu(OH$_2$)(cage)], which released a copper ion by ultraviolet (UV) light irradiation. Click chemistry reaction can be started by using [Cu(OH$_2$)(cage)] with the combination of UV irradiation. When the [Cu(OH$_2$)(cage)] were located the internal aqueous phase of the glycolipid **1** vesicle, the modification was only carried out inner surface of the vesicle by the irradiation of UV light. The specific modification was confirmed by ESI-MS measurement.

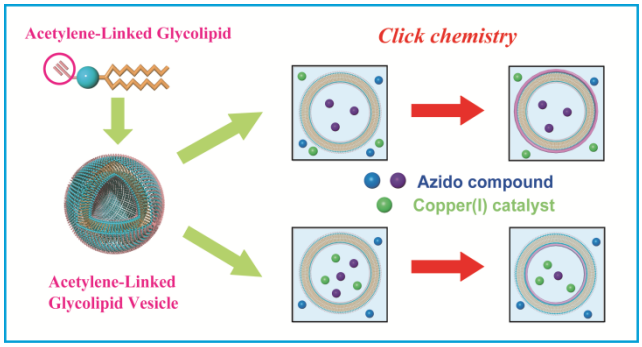

In summary, we succeeded in preparing the acetylene-linked glycolipid **1** vesicles. By using this vesicles combined with the photoresponsible [Cu(OH$_2$)(cage)], we can specifically modify the inner or outer surface of the vesicles.

Next, we will try to prepare a highly efficient photo-energy conversion system using a vesicle lipid bilayer environment. Some glycolipids have an ability to solubilize and stabilize unstable membrane proteins. If the glycolipid **1** vesicles can be used for reconstitution of membrane protein, we can functionalize the glycolipid **1** vesicles by click chemistry in the presence of proteins. For example, photosystem in photosynthetic reaction center is carried out charge separation by the light irradiation. Released electrons are transferred to an electron carrier immobilized on the inner surface of vesicles by click chemistry, and further transferred to another membrane bound enzyme.

As a model for this system, we carried out the photo-oxidization of propylene using chloroplast and membrane fraction containing particle methane monooxygenase (pMMO). By using this system, chloroplast from spinach reduces NAD(P)$^+$ to NAD(P)H by photo-energy. Photoreduced NADH transfers electrons to pMMO through NADH quinone oxidoreductase (NQO) in membrane function from *M. trichosporium* (OB3b), so that pMMO oxidizes propylene to propylene oxide. This is heterogeneous system, so we would like to prepare the electron transfer system in a vesicle lipid bilayer.

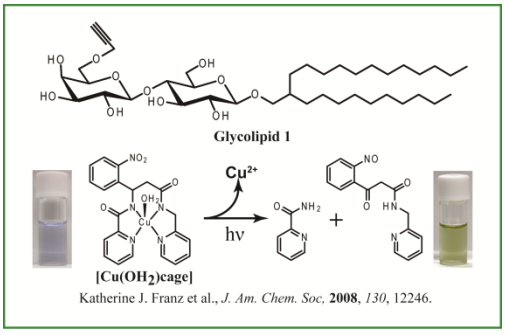

Katherine J. Franz et al., *J. Am. Chem. Soc*, **2008**, *130*, 12246.

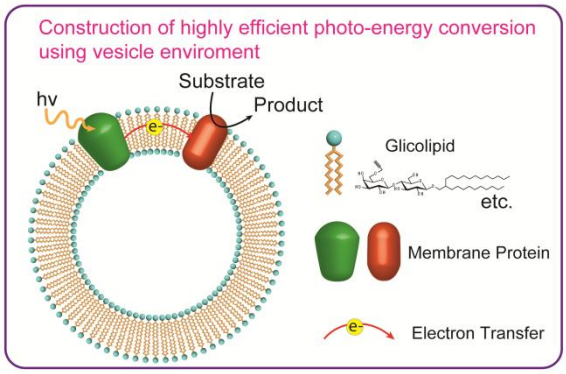

10:55 ～

The initial phase of chromosome condensation requires Cdk1-mediated phosphorylation of the CAP-D3 subunit of condensin II

Nagasaka, Kota

Cluster 1

Back ground

The genome of a cell is duplicated in S phase, and subsequently segregated equally into two daughter cells in mitosis. The cell cycle transition from interphase into mitosis is best characterized by the appearance of condensed chromosomes that become microscopically visible as thread-like structures in nuclei. Mitotic chromosome structure is assumed to be essential for protecting and passing genetic material faithfully to daughter cells. Biochemically, launching the mitotic program requires the activation of the mitotic Cdk1 (cyclin-dependent kinase 1), however, whether and how Cdk1 triggers chromosome assembly at mitotic entry are not well understood.

A large-scale reorganization of chromatin fibers into mitotic chromosomes depends on chromosome condensation mediated mainly by condensin complex. In metazoans, there are two classes of condensin complex, termed condensin I and II, both of complexes accumulate at the chromosome axis and it is thought that they contribute to chromosome condensation by inducing super coiling into DNA. Although two of condensin II are consists of similar components, condensin I and condensin II behave differently from each other and have distinct functions during mitotic chromosome assembly. Especially, condensin II localizes in the nucleus and thus can accumulate at chromosome axes from early stages of prophase. Consistent with this observation, the activity of condensin II is indispensable to initiate chromosome condensation in prophase, however, how condensin II contribute to initiation of chromosome condensation is still unclear.

Specific aim

To address how cells drive chromosome condensation at the entry of mitosis, we focused on condensin II complex and analyzed the regulation condensin II, because condensin II is the only chromosomal component that is known to be essential for timely chromosome condensation in prophase.

Plk1 recognizes CAP-D3 Thr1415 which is Phosphorylated by Cdk1.

Firstly, to address how condensin II is regulated in mitosis, we searched for proteins that bind to condensin II in a mitosis specific manner. As a result, Polo like kinase 1 (Plk1) was found to interact with condensin II. In amino acid sequence of CAP-D3, we identified CAP-D3 Thr1415 as Plk1 binding site through Polo box domain (PBD). Plk1 co-localizes on chromosome axis with condensin II, and this localization of plk1 depends on phosphorylation of the CAP-D3 Thr 1415 residue. CAP-D3 Thr1415 matches not only PBD binding motif but also Cdk1 phosphorylation motif. In vitro kinase assay suggested that CAP-D3 Thr1415 is phophorylated by Cdk1. We also identified CAP-D3 Ser1419 as plk1 phosphorylation site. To confirm these in vivo, we generated antibodies named pT1415 and pS1419, which specifically recognize CAP-D3 when each site is phosphorylated. Immunoblot with these antibodies revealed that treatment of Cdk1 and Plk1 inhibitor suppresses the phosphorylation of Thr1415 and Ser1419, respectively, in cells. These results together indicate that T1415 and S1419 are phosphorylated by Cdk1 and plk1, respectively.

Phosphorylation of CAP-D3 Thr1415 is critical for mitotic function of condensin II.

Secondly, to assess the significance of phospho-regulation of condensin II mediated by Cdk1 and plk1, we generated the condition that a series of cell lines stably expressing WT, T1415A and S1419A mutant were generated and depleted endogenous CAP-D3 by RNAi treatment in the cells. In this experimental condition, we found that prophase chromosome condensation defects due to inactivation of condensin II could be rescued by the expression of WT and S1419A, but not T1415A. However, replacement of not only T1415A, but also S1419A mutant caused curly chromosomal axis (Fig1) and an increasing rate of chromosome segregation failure. These results together suggest that phorsphorylation of CAP-D3 Thr1415 is critical for the early phase of chromosome condensation, and phospho-regulation of condensin II mediated by Cdk1 and plk1 is required for maintaining condensin II function through mitosis.

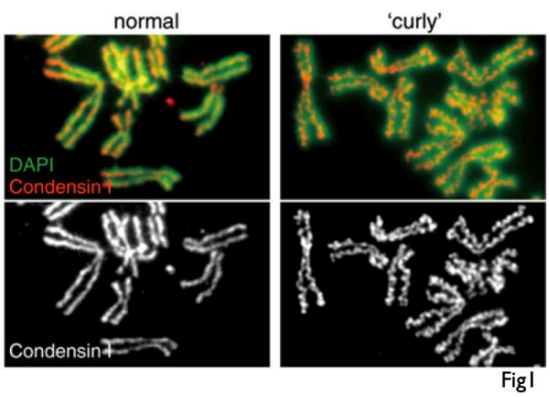

Fig1

Plk1 that accumulate on chromosomal axis induce further phosphorylation to condensin II components.

Finally, we analyzed the phsophorylation levels of whole components of condensin II mediated by Plk1 by using mobility shift of proteins as output. As a result, we found that phosphorylation of each components of condensin II depends on plk1 activity. Additionally, we found that displacement of Plk1 from chromosomal axis due to non-phosphorylatable Thr1415 decreases phosphorylation levels of all of condensin II components mediated by Plk1. This indicates that enrichment of Plk1 on chromosome axis through interaction between plk1 and phosphorylated CAP-D3 Thr1415 is required for efficient phosphorylation of whole condensin II components. Therefore, we propose that the Cdk1-mediated phosphorylation of CAP-D3 Thr 1415 creates a binding module for the PBD, and CAP-D3-bound Plk1 further promotes hyperphosphorylation of the whole condensin II complex, including CAP-D3 itself. (fig2)

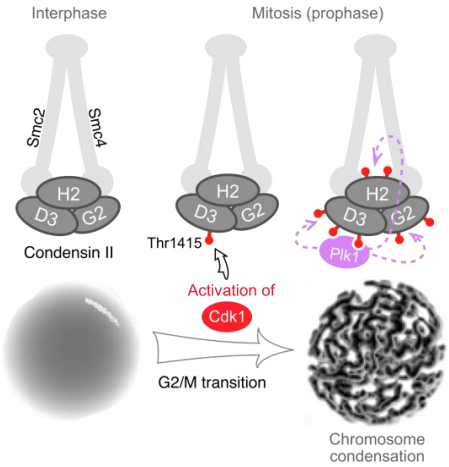

Fig2

Conclusion

In this study, we identified CAP-D3 Thr1415 as a substrate of Cdk1, and this modification is crucial for initiation of chromosome condensation in prophase. This phosphorylation is also critical for efficient regulation of condensin II mediated by Plk1. Defining CAP-D3 as a physiological substrate of Cdk1 provides a molecular explanation for how Cdk1 triggers mitotic chromosome assembly.

11:05 ～

Identification of renal transporters involved in Ca^{2+} and Mg^{2+} excretion by seawater fish

Islam, Zinia

Cluster 1

Marine fish drinks seawater as a major water source which contains ~460 mM Na^+, ~535 mM Cl^-, ~10 mM Ca^{2+}, ~53 mM Mg^{2+} and ~27 mM SO_4^{2-}. The ingested excess divalent ions are excreted by the intestine and by kidney. Seawater (SW) fish form a small amount of isotonic urine that contains a high concentration of divalent ions: 57–167 mM Mg^{2+}, 29–125 mM SO_4^{2-} and 7.5–39 mM Ca^{2+}. In SW fish, the glomerular filtration rate is very low, and the renal excretion of divalent ions is dependent largely on active secretion by renal tubule. Therefore, the SW fish kidney is a good model of renal secretion of divalent ions. Recently, ion transporters that are involved in renal SO_4^{2-} secretion have been identified, but transporters involved in renal Ca^{2+} and Mg^{2+} secretion have yet to be identified. In this study, to identify ion transporters that are involved in renal Ca^{2+} and Mg^{2+} excretion, I analyzed *Takifugu rubripes* (Tiger puffer, Torafugu) and *Takifugu obscurus* (River puffer, Mefugu) as animal model. *T. obscurus* (mefugu) is a useful animal model for studying the mechanism of osmoregulation because 1) it has a strong ability to maintain body fluid homeostasis during adaptation to low and high environmental salinities and is fully adaptable to both freshwater (FW) and SW, 2) *T. rubripes* (torafugu) genome project was completed and the members of the genus Takifugu are very closely related and share ~99% identities in their nucleotide sequences of genes and 3) the nephrons of FW- or SW-acclimated mefugu composed of glomerulus, proximal tubule, distal tubule and collecting duct, while torafugu (SW fish) lacks the distal tubule.

Na^+/Ca^{2+} exchanger (NCX) is a family of proteins that mediate Ca^{2+} efflux from the cell. To identify which NCX is involved in renal Ca^{2+} excretion, tissue distribution of torafugu NCXs was analyzed by RT-PCR. Among seven members of torafugu NCX family, NCX2a was found to be highly and specifically expressed in the SW torafugu kidney. Tissue distribution of NCXs in FW- and SW-acclimated mefugu was also analyzed, and the expression patterns of NCXs were very similar between torafugu and mefugu. NCX2a mRNA markedly increases when mefugu was transferred from FW to SW, suggesting that NCX2a is involved in SW acclimation. In contrast, others reported that NCX2a is not expressed in the kidney of zebrafish, a FW fish. In situ hybridization and Immunohistochemical analyses indicated that NCX2a is expressed in the proximal tubule cells at the apical membrane, where Ca^{2+} excretion is expected to occur in SW fish. When expressed in Xenopus oocytes, NCX2a showed Na^+/Ca^{2+} exchange activity.
These results suggest that NCX2a mediates renal Ca^{2+} secretion at the apical membrane of renal proximal tubules and has an important role in whole body Ca^{2+} homeostasis of marine teleosts.

Next, I focused on the identification of ion transporters that are involved in renal Mg^{2+} secretion. I identified several Mg^{2+} transporter families in SW pufferfish torafugu (*T. rubripes*) by database mining. Among the candidate transporter families, Slc41a1 (solute carrier family 41, member 1) and ACDP3 (ancient conserved domain protein 3) were found to be highly expressed in the SW torafugu kidney and mefugu kidney. Their mRNAs markedly increased when mefugu were transferred from FW to SW. In situ hybridization and immunohistochemical analyses demonstrated that Slc41a1 localizes to the basal plasma membrane and ACDP3 localizes to the lateral plasma membrane in the proximal tubule of SW mefugu. These findings suggest that, Slc41a1 and ACDP3 are strong candidates which are involved in Mg^{2+} secretion by renal proximal tubule of marine teloest.

After the finding that urine of marine teleost fish contain large amounts of Mg^{2+} and Ca^{2+} in 1930s, the molecular mechanisms how Mg^{2+} and Ca^{2+} are secreted and concentrated by renal tubular epithelial cells are still unknown. By using fugu genome database, I identified Ca^{2+} and Mg^{2+} transporters that are highly expressed in renal tubule and propose new epithelial models for Ca^{2+} and Mg^{2+} secretion.

11:15 ～

Characterization of human Smc5/6 complex

Gallego Paez, Lina Marcela

Cluster1

Structural Maintenance of chromosome (SMC) proteins are the core of important protein complexes involved in chromosome structure and segregation. The Cohesin complex holds sister chromosomes together after replication and the Condensin complex compacts the chromosomes at mitosis. The related Smc5/6 complex is also essential and conserved from yeast to humans, and has been found to participate in homologous recombination repair (HRR), rDNA stability and telomere maintenance, although how exactly it regulates these processes to ensure accurate chromosome segregation remains an open question.

We have analyzed the cell cycle profile of EGFP-hSmc5 using time-lapse imaging, revealing that the protein localizes to the nucleus at constant levels until nuclear envelop breakdown in prophase after which the fluorescent signal is diffused through the cytoplasm, being then recovered at the nuclei of daughter cells in early G1 phase. Remarkably, chromatin fractionation assay of hSmc6 showed a similar localization pattern of the protein during the cell cycle, supporting the idea that Smc5/6 complex delocalizes from condensed chromosomes in human cells, a profile that differs from that observed for this complex in other species.

Preliminary results obtained for Chromatin Immunoprecipitation coupled with DNA sequencing (ChIP-Seq) have revealed that hSmc6 protein associates with both intergenic and genic regions during G2 phase and interestingly, about half of the hSmc6 binding sites correspond to cohesin binding sites, implying a possible interplay between these two complexes in the maintenance of sister chromatid cohesion.

Moreover, knockdown of hSmc5 and hSmc6 by RNAi treatment in HeLa and RPE cells generated a variety of chromosome rearrangements, and specially in the case of RPE cells the depletion of hSmc6 caused a clear deficiency in chromosome condensation and resolution of sister chromatid catenations. In the same line of evidence, chromatin fractionation analysis indicated that in the absence of hSmc6, Topo II (which is known as a determinant protein for chromosome condensation and resolution of DNA catenations) delocalize from mitotic chromosomes to the cytoplasmic fraction. All these results are consistent with the notion of hSmc5/6 having a role in DNA damage repair as well as in the maintenance of general chromosome architecture including sister chromatid cohesion and condensation.

Visualization of Mouse Embryonic Stem Cell Cycle with Fucci Proteins on E-cadherin Engineered matrix.

Jovic, Dragomirka

Cluster3

Stem cells have enormous potentiality to differentiate into diverse cell types. Embryonic stem cells represent a good candidate to analyze interactions of correlated proliferation and differentiation process. Understanding the cell cycle restructures is essential for cell-based therapy. Recent studies on stem cell technology facing problems using natural extracellular matrix to visualize individual phases of cell cycles due to the presence of heterogeneous environment. We developed a recombinant E-cadherin substratum that forms single cells without colony formations. Mouse ES cells in a single form are visualized using fluorescente ubiquitination-based cell cycle indicator (Fucci).With dual-color fluorescent probes we were able to indicate whether individual live cells are in G1 phase or S/G2/M phases. The combination of mouse ES cells on E-cadherin substratum and Fucci proteins might be useful for long cell imaging to understand how ES cell cycle is coordinated with various biological events.

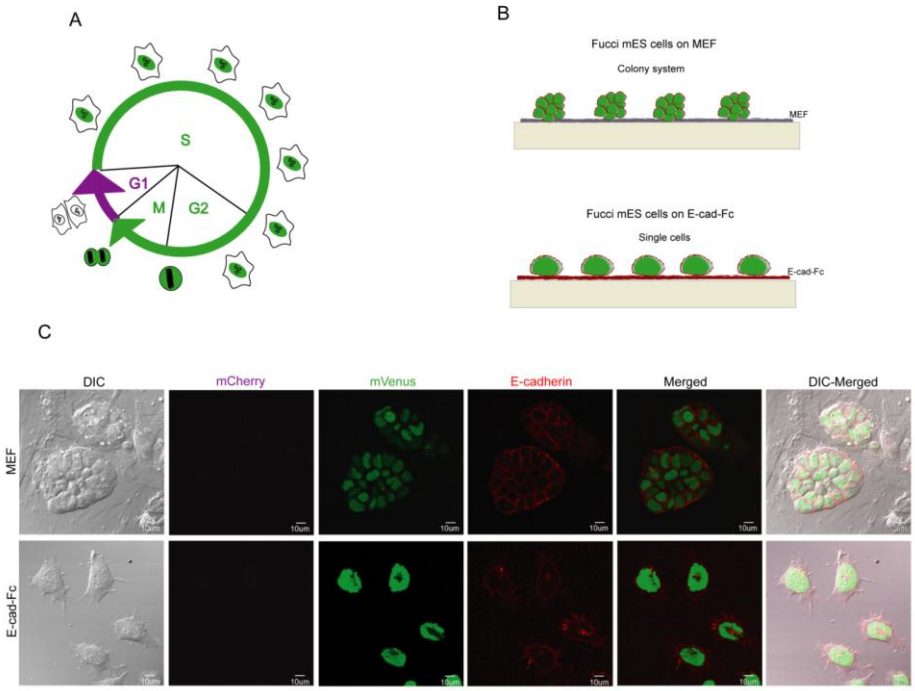

Figure 1 Fucci-signal of mouse embryonic stem cells.

A fluorescent probe that labels individual G1 phase nuclei in red and S/G2/M phase in nuclei green (A). Fucci mouse embryonic stem cells seeded on conventional feeder layers make colonies that unable visualization. However, Fucci mES cells seeded on artificial designed E-cad-Fc matrix shown single cells morphology very convenient to visualize. Schematic representation (B) and Fucci mES cells taken on confocal microscope FV1000D (C).

11:35 ～

pH Robustness mechanism of disulfide-bond formation system in E.coli based on kinetic analyses using QCM

Yazawa, Kenjiro
Cluster2

In the periplasm of *E.coli*, DsbA works as a donor of a disulfide bond to a newly synthesized protein, while DsbB, a plasma membrane protein, re-oxidizes DsbA for catalytic turnover(Fig.1). DsbA has two cysteine residues; Cys30 and Cys33, while DsbB has four cysteine residues; Cys41, Cys44, Cys 104, and Cys130. Oxidation of DsbA by DsbB proceeds as follows(Fig.2). Nucleophilic attack of thiolate of Cys30 in DsbA to Cys104 in DsbB triggers the reaction followed by electron transition to Cys130 in DsbB, then thiolate of Cys130 in DsbB causes an intramolecular nucleophilic reaction to Cys41 and an electron moves to Cys44 in DsbB. Finally, intramolecular nucleophilic attack of Cys33 to Cys30 in DsbA completes the oxidation of DsbA. This reaction between DsbA and DsbB is controlled by a nucleophilic attack of the thiolate anion of the cysteine residue which generally has a pK_a of 8.2, therefore this reaction seems active when reaction condition is in alkaline pH. However, DsbA oxidation by DsbB is maintained from pH 4 to pH 9, with a pH optimum at 6. This feature of the DsbA-DsbB system may be helpful for *E.coli* which survives in various pH conditions because pH of the periplasmic space is variable depending on pH of the outer emvironment. To elucidate this pH robustness mechanism of DsbA-DsbB reactions, we monitored an intermediate complex between DsbA and DsbB in the process of oxidation at various pH as a mass change in real-time using a mass sensor, quartz crystal microbalance (QCM) and obtained pH-dependent kinetic parameters(k_{on}, k_{rev}, k_{off}, and k_{cat}) of the DsbA-DsbB reaction and pH-rate constant profile of them leads to both reaction rates and pK_a of the corresponding cysteine in DsbA and DsbB.

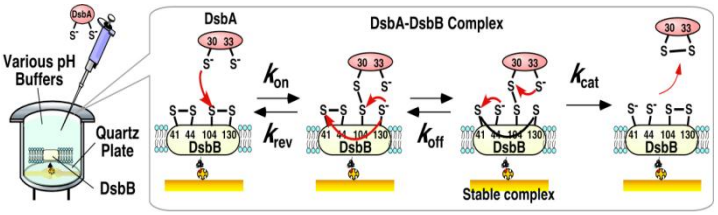

Fig.2. Observation of DsbA-DsbB reactions using QCM method.

QCM charts of the reaction between DsbA and DsbB at various pH are shown in Fig.3. Reaction behavior was different depending on the pH. In the case of pH 5.0 and 6.0, frequency first decreased and then increased due to the binding between DsbA and DsbB followed by intramolecular nucleophilic reaction in DsbA. At pH 4.0, the same behavior was observed as that of pH 5.0 and pH 6.0, however, frequency decrease was smaller. This may be due to the slower binding and dissociation. At pH 3.0, frequency change was not observed, which resulted from the protonation of thiol on Cys30 in DsbA. Obtained kinetic parameters of the DsbA-DsbB reaction using QCM measurements are summarized in Fig 4. The pK_a of k_{on} was 3.5, thus the initial nucleophilic reaction by Cys30 in DsbA to Cys104 in DsbB could proceed even in the acidic condition. The pK_a of k_{off} was 8.0, thus the dissociation reaction derived from intramolecular nucleophilic reaction by Cys44 to Cys41 in DsbB was active in the alkaline condition over pH 8.0. The pK_a of k_{rev} was 6.5, therefore the reverse reaction caused by intramolecular nucleophilic reaction of Cys130 to Cys104 in DsbB was active in the alkaline condition over pH 6.5. The pK_a of k_{cat} was 7, therefore the intramolecular nucleophilic reaction derived from Cys33 in DsbA was active in the range of pH > 7. Oxidation efficiency of DsbA by DsbB(native) was maintained over the pH range from 4 to 8. This pH range was consistent with the pK_a of k_{on} (pK_a 3.5) which drives the forward reaction and k_{off} (pK_a 8) which drives the reverse one respectively. Meanwhile, DsbB(C41A, C44A) had the oxidation activity of DsbA in the pH range from 3 to 6, which corresponds to the k_{on}(pK_a 3.5) and k_{rev}(pK_a 6.5) respectively. From these results, DsbB could form a stable intermediate complex in the process of DsbA oxidation by employing its four cysteines and also shift the pK_a of the reverse reaction from 6.5 to 8.0, thus improves the reaction efficiency and fulfills a role in oxidation of DsbA in the wide pH range.

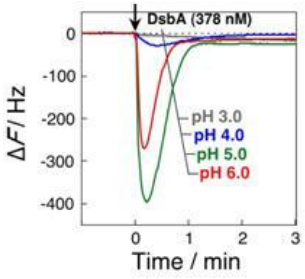

Fig.3. Frequency changes of DsbA-DsbB reactions in various pH conditions. (50 mM Citrate (pH 3.0, 4.0, 5.0 and 6.0), 100 mM NaCl at 25 °C)

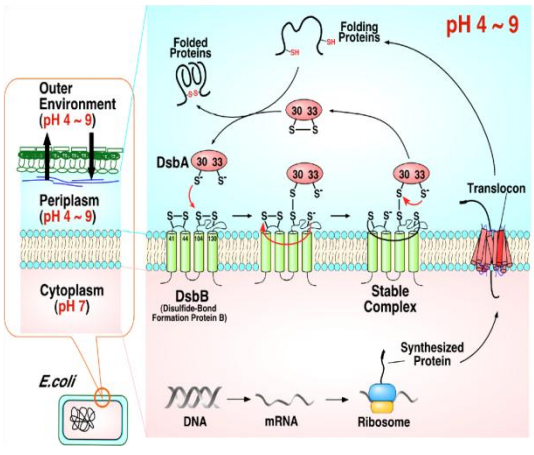

Fig.1. Disulfide-bond formation system in *E.coli* cell.

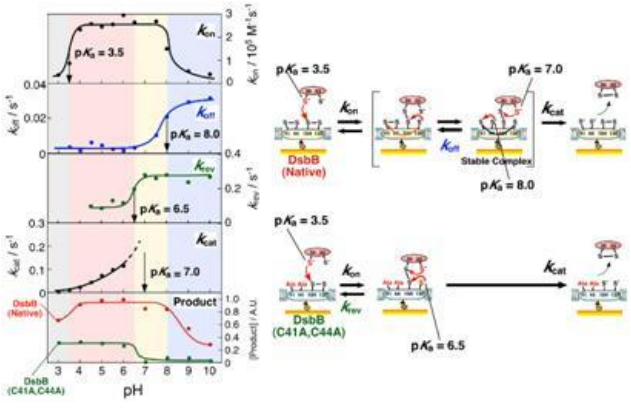

Fig.4. pH-rate profile of DsbA-DsbB reaction using DsbA, DsbB, and DsbB(C41A, C44A).